CrystEngComm

PAPER

Racemic Charge-Transfer Complexes of Helical Polycyclic Aromatic Hydrocarbon Molecule†

Received 00th January 20xx,
Accepted 00th January 20xx

DOI: 10.1039/x0xx00000x

www.rsc.org/

Yukihiro Yoshida,*[ab] Yuto Nakamura,[c] Hideo Kishida,[c] Hiromi Hayama,[a] Yoshiaki Nakano,[bd] Hideki Yamochi[bd] and Gunzi Saito[ae]

Singles crystals of racemic charge-transfer complexes comprising a helical polycyclic aromatic hydrocarbon molecule, [6]helicene, as the electron donor (D) and 7,7,8,8-tetracyano-*p*-quinodimethane (TCNQ) analogs as the electron acceptor (A) were obtained by either co-sublimation or solvent evaporation. All complexes consist of heterochiral DA-type alternating π-columns with a [···(*P*)-[6]helicene···TCNQ···(*M*)-[6]helicene···TCNQ···] repeating unit, which show a peculiar wavy feature primarily related to the nonplanar geometry of [6]helicene molecules. [6]Helicene molecules form a two-dimensional sheet intersecting the columns, and the molecular arrangement (namely, either homochiral or heterochiral arrangement) in the sheets depends on the TCNQ analog. Theoretical calculations were carried out to discuss the origin of the molecular deformation of [6]helicene molecules in the CT solids in terms of intermolecular interactions.

Introduction

For more than half a century, polycyclic aromatic hydrocarbons (PAHs) have been widely utilised in organic electronics, e.g., photovoltaics, field-effect transistors, and solar cells.[1–3] Intermolecular π-π interactions promote the self-assembly of PAH molecules into columnar stacks; therefore, these interactions play a crucial role in the π-electronic properties of the aggregates. Furthermore, co-crystallization with electron-donating (D) or -accepting (A) counter molecules, with diverse combinations, utilizing charge-transfer (CT) interactions has afforded a variety of exotic PAH-based electronic materials, e.g., metals and superconductors.[4–6]

Recently, nonplanar π-conjugated molecules have attracted attention as components for the assembly of an unconventional π-electron network.[7–9] Two main approaches are utilised to produce nonplanar PAH molecules: endoskeletal and exoskeletal approaches. In the former approach, a nonhexagonal ring is present inside hexagonal skeletons (e.g., [*n*]circulenes;[10] Scheme 1a), while the latter approach exploits steric hindrance because of crowdedness (e.g., [*n*]helicenes;[11,12] Scheme 1b). With respect to the former type, our group has reported the first corannulene-based CT solid using 7,7,8,8-tetracyano-*p*-quinodimethane (TCNQ; Scheme 1c), (corannulene)$_2$TCNQ; in this solid, the CT interaction with an adjacent TCNQ molecule on the convex side of the corannulene is apparently greater than that on the concave side.[13] In this study, four racemic CT complexes based on [6]helicene, which is categorised into the latter group, were prepared using various TCNQ analogs (Scheme 1c–1f), and their optical and crystallographic properties, in addition to theoretical calculations, were investigated. For [*n*]helicenes, increasing efforts continue to be devoted to achieving control crystalline forms of racemates, i.e., racemic mixtures (conglomerates), racemic compounds, or solid solutions, by changing molecular structures, counter components, and crystallization processes.[11,12]

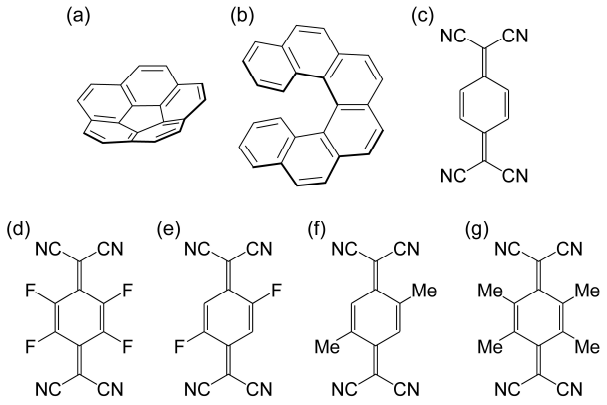

Scheme 1 Molecular structures of (a) corannulene ([5]circulene), (b) [6]helicene, (c) TCNQ, (d) F_4TCNQ, (e) F_2TCNQ, (f) Me_2TCNQ, and (g) Me_4TCNQ.

Results and Discussion

Crystal Growth

Commercial racemic [6]helicene was used as received. CT complexes with TCNQ analogs, ([6]helicene)(F_4TCNQ) (**1**), ([6]helicene)(F_2TCNQ) (**2**), and ([6]helicene)(Me_2TCNQ) (**4**), were prepared by co-sublimation, whereas a CT complex with parent

[a] Faculty of Agriculture, Meijo University, Nagoya 468-8502, Japan; E-mail: yyoshida@meijo-u.ac.jp
[b] Division of Chemistry, Graduate School of Science, Kyoto University, Kyoto 606-8502, Japan
[c] Department of Applied Physics, Nagoya University, Nagoya 464-8603, Japan
[d] Research Center for Low Temperature and Materials Sciences, Kyoto University, Sakyo-ku, Kyoto 606-8501, Japan
[e] Toyota Physical and Chemical Research Institute, Nagakute 480-1192, Japan

† Electronic Supplementary Information (ESI) available: Infrared spectra and X-ray crystallographic data in CIF format for **1**–**4**. See DOI: 10.1039/x0xx00000x

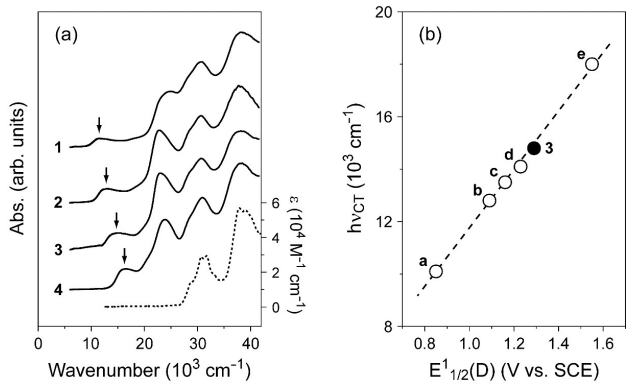

Fig. 1 (a) Electronic absorption spectra of **1**–**4** measured on KBr pellets (solid lines) together with pristine [6]helicene in a 10^{-5} M chloroform solution (dotted line). Arrows denote the CT absorption bands. (b) Plot of CT energy ($h\nu_{CT}$) against the first redox potential of PAH molecules ($E^1_{1/2}$(D)) in the TCNQ complexes (**a**: (perylene)(TCNQ),[17] **b**: (anthracene)(TCNQ),[18] **c**: (pyrene)(TCNQ),[19] **d**: (coronene)(TCNQ),[20,21] **e**: (triphenylene)$_2$(TCNQ)(toluene)[22]).

TCNQ, ([6]helicene)(TCNQ) (**3**),[14] was prepared by solvent evaporation (see Experimental section). Notably, co-sublimation and solvent evaporation using Me$_4$TCNQ (Scheme 1g) with a weak electron-accepting ability ($E^1_{1/2}$(A) = –0.05 V vs. saturated calomel electrode (SCE)) afforded no trace of the CT complex.

Charge Transfer

Fig. 1a shows the electronic absorption spectra of **1**–**4** dispersed in KBr pellets. A low-lying band, corresponding to the intermolecular CT transition, was observed at $h\nu_{CT}$ = 11–17 × 10^3 cm^{-1} in addition to the intramolecular transition bands of the component molecules at greater than 20 × 10^3 cm^{-1}. The low-energy band provides clear evidence of the CT interactions between [6]helicene and TCNQ analogs in solids. The $h\nu_{CT}$ value steadily decreases with the increase in the electron-accepting ability of the TCNQ analogs (Table 1). This relationship is indicative of a neutral ground state with alternating π-columns,[15] which is in agreement with the high first redox potential of [6]helicene ($E^1_{1/2}$(D) = 1.29 V vs. SCE[16] relative to the $E^1_{1/2}$(A) values of the TCNQ analogs. Notably, complex **3** formed with parent TCNQ lies on a straight line via the application of a least-squares method to the plots of $h\nu_{CT}$ against $E^1_{1/2}$(D) of typical planar PAH

Table 1 Typical parameters for **1**–**4**

Complex	**1**	**2**	**3**	**4**	(*M*)-[6]helicene
Acceptor (A)	F_4TCNQ	F_2TCNQ	TCNQ	Me_2TCNQ	—
$E^1_{1/2}$(A) (V vs. SCE)[a]	0.60	0.41	0.22	0.15	—
$h\nu_{CT}$ (10^3 cm^{-1})[b]	11.6	12.9	14.8	16.5	—
d (Å)[c]	4.39	4.20	4.19, 4.20	4.12	4.48
γ (°)[d]	57.6	47.0	45.1, 46.2	41.8	59.5

[a] First redox potential of TCNQ analogs (SCE: saturated calomel electrode). [b] CT absorption band measured on KBr pellets. [c] Distance between the terminal benzene centroids in a [6]helicene molecule based on the crystallographic data at 100 K. [d] Angle between the planes of the terminal benzene rings in a [6]helicene molecule based on the crystallographic data at 100 K.

Table 2 Crystallographic data of **1**–**4**

Complex	**1**	**2**	**3**	**4**	(*M*)-[6]helicene
Formula	$C_{38}H_{16}F_4N_4$	$C_{38}H_{18}F_2N_4$	$C_{38}H_{20}N_4$	$C_{40}H_{24}N_4$	$C_{26}H_{16}$
Formula weight	604.57	568.58	532.60	560.66	328.41
Crystal system	Orthorhombic	Monoclinic	Monoclinic	Monoclinic	Orthorhombic
Space group	*Pbcn*	$P2_1/n$	$P2_1/c$	$C2/c$	$P2_12_12_1$
Crystal size, mm^3	0.37 × 0.32 × 0.10	0.38 × 0.19 × 0.11	0.47 × 0.06 × 0.05	0.49 × 0.46 × 0.40	0.36 × 0.24 × 0.06
a, Å	7.1454(4)	8.3747(4)	8.2077(5)	14.4593(7)	7.3079(3)
b, Å	17.2601(9)	16.7659(8)	33.7880(19)	11.4032(6)	12.9491(6)
c, Å	22.2970(11)	19.2823(9)	19.3173(11)	17.8273(9)	17.4393(8)
α, deg	90	90	90	90	90
β, deg	90	90.488(1)	92.882(1)	102.652(1)	90
γ, deg	90	90	90	90	90
V, Å^3	2749.9(3)	2707.3(2)	5350.3(5)	2868.0(3)	1650.3(1)
Z	4	4	8	4	4
Temperature, K	100	100	100	100	100
d_{alc}, g cm^{-3}	1.460	1.395	1.322	1.298	1.322
μ(Mo Kα), mm^{-1}	0.106	0.093	0.079	0.077	0.075
Reflns used	2811	5528	10950	2929	3371
Refined params	209	404	757	201	235
R_1 (for $I > 2\sigma(I)$)[a]	0.0321	0.0391	0.0482	0.0343	0.0294
wR_2 (for all data)[b]	0.0915	0.0991	0.1045	0.1016	0.0724
GOF on F^2	1.045	1.019	0.975	1.096	1.058
CCDC number	1533425	1533426	1533427	1533428	1535631

[a] $R_1 = \Sigma(||F_o| - |F_c||)/\Sigma|F_o|$. [b] $wR_2 = [\Sigma w(F_o^2 - F_c^2)^2/\Sigma w(F_o^2)^2]^{0.5}$.

molecules (perylene,[17] anthracene,[18] pyrene,[19] coronene,[20,21] and triphenylene[22]) for their TCNQ complexes (Fig. 1b).

Infrared spectra of **1**–**4** are readily assigned by the superposition of those of the component molecules, which also supports the neutral ground state (Fig. S1 in ESI†). For complex **1** formed with the strongest electron acceptor, F_4TCNQ, the b_{1u} $\nu_{C=C}$ mode (1591 cm^{-1}) is shifted to a low frequency by 9 cm^{-1} relative to that of neutral F_4TCNQ (1600 cm^{-1}). Assuming that the reduction state of F_4TCNQ molecule is linearly correlated with the $\nu_{C=C}$ shift, namely $\delta = -(\omega_{obs} - \omega_o)/(\omega_1 - \omega_0)$, where ω_{obs}, ω_0, and ω_1 denote the $\nu_{C=C}$ mode frequencies of a CT complex, neutral F_4TCNQ, and monoanionic F_4TCNQ, respectively,[23] the charge of the F_4TCNQ molecules in **1** was estimated to be as low as approximately –0.1.

Crystal Structure

Crystal structures of **1**–**4** were determined at 100 K (Table 2). Despite their distinct crystal lattices, all complexes exhibit 1:1 stoichiometry, with peculiar wavy DA-type alternating π-columns. In the column, [6]helicene and TCNQ analogs are arranged in a heterochiral manner, with a [···(*P*)-[6]helicene···TCNQ···(*M*)-[6]helicene···TCNQ···] repeating unit. These complexes are racemates, and no spontaneous enantiomer resolution occurred during crystallization. Complex **3** prepared in this study exhibits a structure identical to that reported by Ermer:[13] two [6]helicene and two TCNQ molecules are crystallographically independent, and the charges of the TCNQ molecules were estimated to be –0.15(4) and –0.12(3) on the basis of the intramolecular bond lengths.[24]

Complex **1** belongs to the orthorhombic system with space group *Pbcn*, and the asymmetric unit contains a half [6]helicene and a half F_4TCNQ. Adjacent (*P*)-[6]helicene and (*M*)-[6]helicene within the column are related by an inversion centre, whereas F_4TCNQ is located on an inversion centre. Distance between the terminal benzene centroids (*d*) and angle between the planes of the terminal benzene rings (*γ*) in [6]helicene were estimated as 4.39 Å and 57.6°, respectively. The contraction of [6]helicene molecules in **1** relative to those in the enantiomeric crystal (4.48 Å and 59.5°, respectively; Table 2)[25,26] is possibly related to Wallach's rule,[27,28] which suggests denser packing in racemic crystals compared to their chiral conglomerates. From bond length analysis,[24,29] the charge of F_4TCNQ was estimated as –0.05(3), which is in good agreement with that expected from the infrared spectrum (*ca.* –0.1).

The complex involves wavy DA-type alternating π-columns along the *c* axis (Fig. 2a). In the column, a terminal benzene ring of [6]helicene and a quinonoid ring of F_4TCNQ exhibits a ring-over-bond overlap pattern (Fig. 2b), and are arranged in a nonparallel fashion with a dihedral angle of 3.98°. At $z \sim 0.25$ and 0.75, [6]helicene molecules form heterochiral sheets comprising equimolar amounts of (*P*)-[6]helicene and (*M*)-[6]helicene. Each F_4TCNQ molecule is connected to two adjacent [6]helicene molecules (one (*P*)-[6]helicene and one (*M*)-[6]helicene) through C–H···F hydrogen bonds (H7···F1: 2.61 Å, H8···F1: 2.48 Å vs. sum of van der Waals radii: 2.67 Å;[30] Fig. 2c) along the molecular short axis to form an infinite array along the [4 0 1] or [4 0 $\bar{1}$] direction. In addition, each F_4TCNQ molecule interacts with two adjacent [6]helicene molecules (one (*P*)-[6]helicene and one (*M*)-[6]helicene) along the molecular long axis through C–H···N hydrogen bonds (H1···N2: 2.55 Å vs. sum of van der Waals radii: 2.75 Å[30]). As shown in Fig. 2d, the hydrogen-bonding interactions afford an infinite supramolecular helix with a [···(*P*)-[6]helicene···F_4TCNQ···(*M*)-[6]helicene···F_4TCNQ···] repeating unit of 26.5 Å along the [2 0 1] or [2 0 $\bar{1}$] direction.

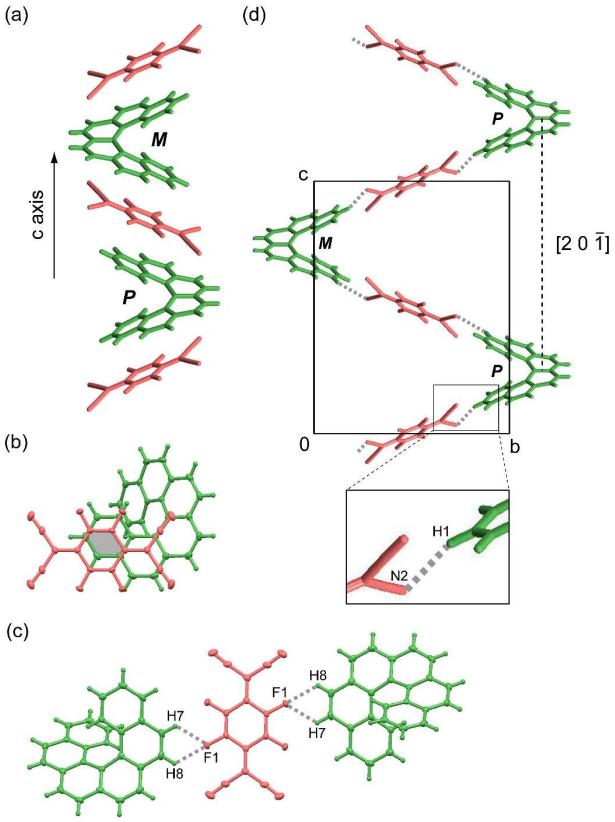

Fig. 2 (a) DA-type alternating π-column in **1** viewed along the *a* axis, where ***P*** and ***M*** indicate (*P*)- and (*M*)-[6]helicene molecules, respectively. (b) Overlap pattern of adjacent [6]helicene and F_4TCNQ within a column viewed perpendicular to the molecular plane of F_4TCNQ in **1**. See text for the grey area. (c) Short C–H···F contacts with H···F distances of less than the sum of the van der Waals radii (2.67 Å; grey dotted lines) around one F_4TCNQ molecule in **1**. (d) Supramolecular helix through C–H···N hydrogen bonds (grey dotted lines) viewed along the *a* axis, where a helix extending along the [2 0 $\bar{1}$] direction is shown. [6]Helicene and F_4TCNQ molecules are shown in green and red, respectively.

Complex **2** crystallises in a monoclinic lattice with space group $P2_1/n$, and each of [6]helicene and F_2TCNQ is crystallographically independent. The *d* and *γ* values of [6]helicene were estimated as 4.20 Å and 47.0°, respectively, and fluorine atoms in F_2TCNQ were orientationally disordered over two distinct orientations, 2,5- and 3,6-positions, with an occupancy ratio of 93/7.

The wavy alternating π-columns shown in Fig. 3a run along the [1 0 1] direction. Each F_2TCNQ exhibits a ring-over-ring overlap with a second terminal benzene ring of [6]helicene with a dihedral angle of 2.32° on one side, whereas it exhibits a ring-over-bond overlap on the other side (Fig. 3b). Unlike **1**, [6]helicene molecules in **2** form homochiral sheets at $z \sim 0.25$ and 0.75 for (*P*)- and (*M*)-type enantiomers, respectively, which are related by an inversion centre. Whereas fluorine atoms in F_2TCNQ form no short interatomic contacts with adjacent [6]helicene molecules in contrast to **1**, intermolecular C–H···N hydrogen bonds (H7···N1: 2.71 Å,

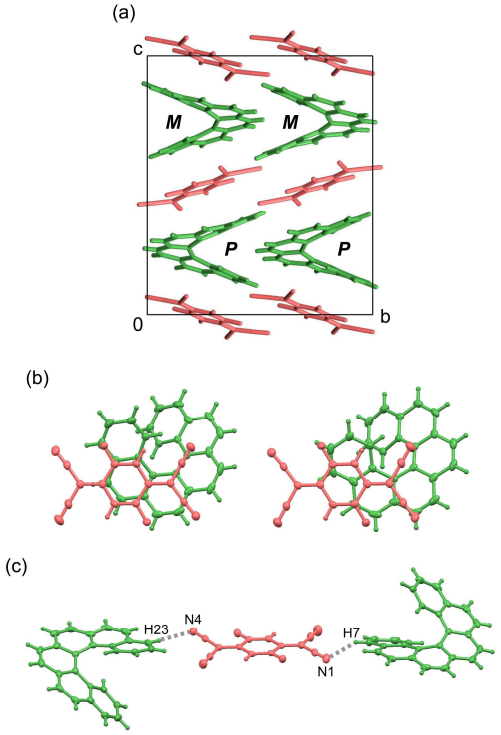

Fig. 3 (a) Crystal structure of **2** viewed along the *a* axis, where ***P*** and ***M*** indicate (*P*)- and (*M*)-[6]helicene molecules, respectively. (b) Overlap pattern of adjacent [6]helicene and F_2TCNQ within a column viewed perpendicular to the molecular plane of F_2TCNQ in **2**. (c) Short C–H···N contacts with H···N distances of less than the sum of the van der Waals radii (2.75 Å; grey dotted lines) around one F_2TCNQ molecule in **2**. Only the major orientation of the disordered F_2TCNQ is shown, and [6]helicene and F_2TCNQ molecules are shown in green and red, respectively.

H23···N4: 2.57 Å; Fig. 3c) result in the formation of an infinite supramolecular helix with a [···(*P*)-[6]helicene···F_2TCNQ···(*M*)-[6]helicene···F_2TCNQ···] repeating unit of 31.5 Å along the [3 0 1] or [3 0 $\bar{1}$] direction.

Complex **4** also belongs to the monoclinic system with space group *C*2/*c*, and the asymmetric unit contains a half [6]helicene and a half Me_2TCNQ. Adjacent (*P*)-[6]helicene and (*M*)-[6]helicene within the column are related by an inversion centre and form homochiral sheets at $z \sim 0.25$ and 0.75, respectively. Notably, the lowest *d* and *γ* values (4.12 Å and 41.8°, respectively) were observed.

The wavy alternating π-columns (pink area in Fig. 4a) run along the *c* axis, in which adjacent [6]helicene and Me_2TCNQ molecules exhibit a ring-over-bond overlap fashion (Fig. 4b). In contrast to other complexes, a bulky methyl group in Me_2TCNQ, which is located on an inversion centre, approaches the adjacent helical core, affording close packing (Fig. 4c). As indicated by the blue area in Fig. 4a, this complex forms infinite supramolecular helices with a [···(*P*)-[6]helicene···Me_2TCNQ···(*M*)-[6]helicene···Me_2TCNQ···] repeating unit of 17.8 Å through C–H···N hydrogen bonds (H1···N1: 2.64 Å). Adjacent helices along the *a* axis are connected through another C–H···N hydrogen bonds (H7···N1: 2.60 Å). Considering that the helices run along the *c* axis, each of the [6]helicene and Me_2TCNQ molecules within the column comprises the same helix.

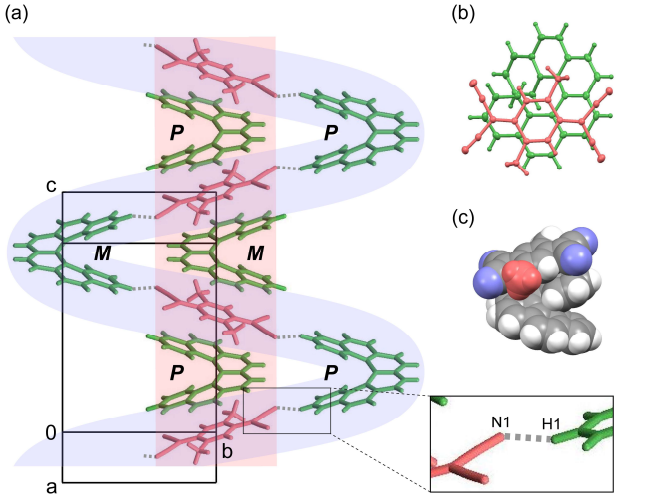

Fig. 4 (a) Crystal structure of **4**, where ***P*** and ***M*** indicate (*P*)- and (*M*)-[6]helicene molecules, respectively. Pink and blue areas denote the DA-type alternating π-column and supramolecular helix, respectively, both of which run along the *c* axis. Grey dotted lines denote C–H···N hydrogen bonds. (b) Overlap pattern of adjacent [6]helicene and Me_2TCNQ within a column viewed perpendicular to the molecular plane of Me_2TCNQ in **4**. (c) Molecular packing of a pair of [6]helicene and Me_2TCNQ molecules, where a methyl group near the [6]helicene molecule is indicated in red. [6]Helicene and Me_2TCNQ molecules in (a) and (b) are shown in green and red, respectively.

Molecular deformation

Thus far, the molecular geometry of [6]helicene has been modified via the coordination of a silver(I) ion[31] and the functionalization of terminal benzene rings.[32] Fig. 5 shows the plots of *d* and *γ* values as a function of the $E^1_{1/2}$(A) values of TCNQ analogs for **1**–**4**. The [6]helicene molecules are seemingly elongated with the increase in the electron-accepting ability of TCNQ analogs; namely, intermolecular CT interactions exhibit beneficial effects on the molecular geometry of [6]helicene in the solid state. However, our density functional theory (DFT) calculations at the CAM-B3LYP-D3(BJ)/spAug-cc-pVDZ level of theory predicted that the cationization of *C*2-symmetric [6]helicene marginally affects molecular geometry; the *d* and *γ* values of the [6]helicene monocation (4.21 Å and 47.2°, respectively) are similar to those of neutral [6]helicene (4.25 Å and 48.5°, respectively).

To help understand the molecular deformation experimentally observed, we turn to the relative configuration between the benzene ring(s) of [6]helicene and a quinonoid ring of TCNQ analogs. In complex **4**, a methyl group of Me_2TCNQ penetrates the helical core of an adjacent [6]helicene within the column, and a hydrogen atom in the methyl group forms a C–H···π hydrogen bond[33,34] at a distance of 2.92 Å with a benzene ring of [6]helicene. Such a complementary interaction inevitably plays an important role in the close packing, possibly leading to the decreased *d* and *γ* values. On the other hand, the increased *d* and *γ* values in **1** are possibly related to the overlap ratio, which is defined as the ratio of the overlap area to the area of a quinonoid ring area viewed perpendicular to the molecular plane of TCNQ analogs (For example, a grey area shown in Fig. 2b); the

overlap ratio in **1** (54%) is apparently less than those in **2** (58%) and **3** (60 and 61%). Although the factors that determine the overlap mode in these solids remain unclear, the depressed intermolecular π-π interactions between [6]helicene and F_4TCNQ molecules within the column possibly result in the elongation of [6]helicene molecules in **1**.

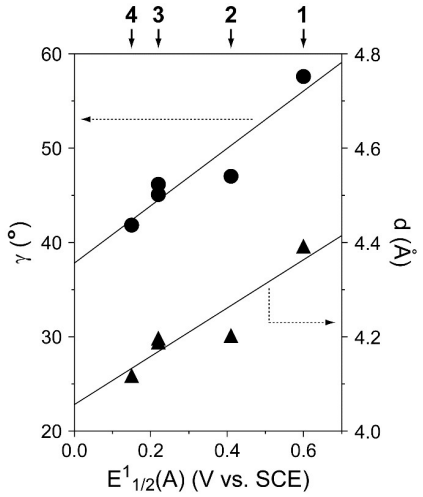

Fig. 5 Plots of distance between the terminal benzene centroids (*d*; triangle) and angle between the planes of the terminal benzene rings (*γ*; circle) in a [6]helicene molecule against the first redox potential of the TCNQ analogs ($E^1_{1/2}$(A)). Solid lines denote the least-square fits of the data.

Conclusions

The combination of racemic [6]helicene and TCNQ analogs yields racemic neutral CT complexes instead of chiral conglomerates. All complexes consist of heterochiral DA-type alternating π-columns with a wavy structure associated with the helical structure of [6]helicene. The small π-π overlap between the adjacent [6]helicene and F_4TCNQ results in the elongation of [6]helicene, whereas the complementary interactions via C–H···π hydrogen bonds between [6]helicene and Me_2TCNQ within the column contracts [6]helicene. Further studies will be focused on the exploration of ionic CT complexes formed with (partially) cationic [6]helicene molecules not only to construct an unprecedented higher-dimensional π-conduction network but also to elucidate the relationship between the molecular geometry of [6]helicene and electronic properties of the CT solids.

Experimental section

General details

1,1,2-Trichloroethane and chloroform were distilled from CaH_2 prior to use. Racemic [6]helicene (Lach-Ner, Czech Republic) was used as received, whereas TCNQ analogs were purified by recrystallization and/or sublimation after being synthesised by our research group or purchased commercially.

Syntheses of 1, 2, and 4

Equimolar amounts of racemic [6]helicene (0.015 mmol) and the TCNQ analog (0.015 mmol) were ground together in an agate mortar and transferred into a borosilicate glass tube with a diameter of 12 mm. After sealing under vacuum (5×10^{-5} Torr), the 13-cm-long tube was placed in a two-zone furnace with a temperature gradient from 201 °C (sample side) to 149 °C (opposite side). After heating for 2–4 days, black thick plate crystals of **1**, black hexagonal bifrustum crystals of **2**, and black block crystals of **4** were grown on the opposite side in the tube. Yield: 30–50%.

Synthesis of 3

Black rod crystals of **3** were obtained by the slow evaporation of a 1,1,2-trichloroethane solution (10 mL) containing equimolar amounts of racemic [6]helicene (0.01 mmol) and TCNQ (0.01 mmol). Yield: ca. 80%.

Spectroscopy

UV-Vis-NIR absorption spectra were measured on KBr pellets (3.8–42×10^3 cm^{-1}) or in a chloroform solution (12–50×10^3 cm^{-1}) using a Shimadzu UV-3100 spectrophotometer. Infrared transmission spectra were measured on KBr pellets using a Shimadzu Prestige-21 spectrophotometer (380–7800 cm^{-1}).

X-Ray structural analysis

Single-crystal X-ray diffraction experiments were performed on a CCD-type diffractometer (Bruker SMART APEX II) with graphite-monochromated Mo Kα radiation (λ = 0.71073 Å) at 100 K. A single crystal was mounted on a glass capillary and cooled by a stream of cooled nitrogen gas. The crystal structures solved by a direct method using the SIR2004 program[35] were refined by a full-matrix least-squares method on F^2 using SHELXL.[36] All non-hydrogen atoms were anisotropically refined. The positional parameters of the hydrogen atoms were calculated under the assumption of fixed C–H bond lengths of 0.93 and 0.96 Å with sp^2 and sp^3 configurations, respectively, of the parent atoms. In the refinement procedures, isotropic temperature factors with a magnitude 1.2-fold greater than that of the equivalent temperature factors of the parent atoms were applied to the hydrogen atoms.

Computational details

DFT calculations were performed using the CAM-B3LYP,[37] CAM-B3LYP-D3(BJ),[37,38] and M11[39] functionals in combination with the spAug-cc-pVDZ basis set.[40,41] Full geometry optimization, with "Opt = Tight" specified, was conducted for C_2-symmetric (*P*)-[6]helicene^0 as well as C_2- and C_1-symmetric (*P*)-[6]helicene$^{\bullet+}$. Note that all of the functionals found one imaginary frequency in C_2-symmetric (*P*)-[6]helicene$^{\bullet+}$, indicating a transition state. The stability of the wave function was confirmed by specifying the "Stable=Opt" keyword. The "Int=SuperFineGrid" keyword was specified throughout the current DFT calculations. All computations were performed with the Gaussian 09 program package.[42]

Acknowledgements

This work was supported by the Japan Society for the Promotion of Science (JSPS) KAKENHI Grant Numbers JP25288041, JP26288035, JP15K17901, JP16H00964, and JP16H04139. Theoretical calculations were performed at the Research Center for Computational Science, Okazaki, Japan, and under the Collaborative

Research Program for Young Scientists at Academic Center for Computing and Media Studies, Kyoto University.

References

1 *Organic Electronics: Materials, Manufacturing, and Applications*, ed. H. Klauk, Wiley-VCH, Weinheim, 2006.
2 F. S. Kim, G. Ren and S. A. Jenekhe, *Chem. Mater.*, 2011, **23**, 682–732.
3 C. Wang, H. Dong, W. Hu, Y. Liu and D. Zhu, *Chem. Rev.*, 2012, **112**, 2208–2267.
4 M. Almeida and R. T. Henriques, *in Handbook of Organic Conductive Molecules and Polymers*, ed. H. S. Nalwa, Wiley, New York, Vol. 1, pp.87–149, 1997.
5 D. Graf, J. S. Brooks, M. Almeida, J. C. Dias, S. Uji, T. Terashima and M. Kimata, *Europhys. Lett.*, 2009, **85**, 27009−27013.
6 G. A. Artioli and L. Malavasi, *J. Mater. Chem. C*, 2014, **2**, 1577−1584.
7 R. Rieger and K. Müllen, *J. Phys. Org. Chem.*, 2010, **23**, 315–325.
8 Y. Segawa, H. Ito and K. Itami, *Nat. Rev. Mater.*, 2016, **1**, 15002.
9 T. Fujikawa, Y. Segawa and K. Itami, *J. Am. Chem. Soc.*, 2016, **138**, 3587–3595.
10 *Fragments of Fullerenes and Carbon Nanotubes: Designed Synthesis, Unusual Reactions, and Coordination Chemistry*, ed. M. A. Petrukhina and L. T. Scott, Wiley, Hoboken, 2012.
11 Y. Shen and C.-F. Chen, *Chem. Rev.*, 2012, **112**, 1463–1535.
12 M. Gingras, G. Félix and R. Peresutti, *Chem. Soc. Rev.*, 2013, **42**, 1007–1050.
13 Y. Yoshida, K. Isomura, Y. Nakamura, H. Kishida and G. Saito, *Chem. Lett.*, 2015, **44**, 709–711.
14 O. Ermer and J. Neudörfl, *Helv. Chim. Acta*, 2001, **84**, 1268–1313.
15 J. B. Torrance, J. E. Vazquez, J. J. Mayerle and V. Y. Lee, *Phys. Rev. Lett.*, 1981, **46**, 253–257.
16 J. W. Diesveld, J. H. Borkent and W. H. Laarhoven, *Reel. Trav. Chim.*, 1980, **99**, 391–394.
17 I. J. Tickle and C. K. Prout, *J. Chem. Soc., Perkin Trans. 2*, 1973, 720–723.
18 R. M. Williams and S. C. Wallwork, *Acta Cryst.*, 1968, **B24**, 168–174.
19 C. K. Prout, I. J. Tickle and J. D. Wright, *J. Chem. Soc., Perkin Trans. 2*, 1973, 528–530.
20 X. Chi, C. Besnard, V. K. Thorsmlle, V. Y. Butko, A. J. Taylor, T. Siegrist and A. P. Ramirez, *Chem. Mater.*, 2004, **16**, 5751–5755.
21 Y. Yoshida, Y. Shimizu, T. Yajima, G. Maruta, S. Takeda, Y. Nakano, T. Hiramatsu, H. Kageyama, H. Yamochi and G. Saito, *Chem. Eur. J.*, 2013, **19**, 12313–12324.
22 Y. Yoshida *et al.* unpublished data.
23 S. Horiuchi, R. Kumai, Y. Okimoto and Y. Tokura, *Chem. Phys.*, 2006, **325**, 78–91.
24 T. J. Kistenmacher, T. J. Emge, A. N. Bloch and D. O. Cowan, *Acta Crystallogr. B*, 1982, **38**, 1193–1199.
25 B. S. Green and M. Knossow, *Science*, 1981, **214**, 795–797.
26 S. Ramdas, J. M. Thomas, M. E. Jordan and C. J. Eckhardt, *J. Phys. Chem.*, 1981, **85**, 2421–2425.
27 O. Wallach, *Justus Liebigs Ann. Chem.*, 1895, **286**, 90–143.
28 C. P. Brock, W. B. Schweizer and J. D. Dunitz, *J. Am. Chem. Soc.*, 1991, **113**, 9811–9820.
29 B. Mahns, O. Kataeva, D. Islamov, S. Hampel, F. Steckel, C. Hess, M. Knupfer, B. Büchner, C. Himcinschi, T. Hahn, R. Renger and J. Kortus, *Cryst. Growth Des.*, 2014, **14**, 1338–1346.
30 A. Bondi, *J. Phys. Chem.*, 1964, **68**, 441–451.
31 E. Makrlík, J. J. Dytrtová, P. Vaňura, I. Císařová, J. Sýkora, V. Církva, J. Storch and M. Polášek, *Struct. Chem.*, 2016, **27**, 627–635.
32 C. Wachsmann, E. Weber, M. Czugler and W. Seichter, *Eur. J. Org. Chem.*, 2003, **2003**, 2863–2876.
33 D. Braga, F. Grepioni and E. Tedesco, *Organometallics*, 1998, **17**, 2669–2672.
34 M. Nishio, *CrystEngComm*, 2004, **6**, 130–158.
35 M. C. Burla, R. Caliandro, M. Camalli, B. Carrozzini, G. L. Cascarano, L. De Caro, C. Giacovazzo, G. Polidori and R. Spagna, *J. Appl. Crystallogr.*, 2005, **38**, 381–388.
36 G. M. Sheldrick, *SHELXL-2013*, University of Göttingen, Germany, 2013.
37 T. Yanai, D. Tew and N. Handy, *Chem. Phys. Lett.*, 2004, **393**, 51–57.
38 S. Grimme, S. Ehrlich and L. Goerigk, *J. Comp. Chem.*, 2011, **32**, 1456–1465.
39 R. Peverati and D. G. Truhlar, *J. Phys. Chem. Lett.*, 2011, **2**, 2810–2817.
40 T. H. Dunning, Jr., *J. Chem. Phys.*, 1989, **90**, 1007–1023.
41 R. A. Kendall, T. H. Dunning, Jr. and R. J. Harrison, *J. Chem. Phys.*, 1992, **96**, 6796–6806.
42 M. J. Frisch, G. W. Trucks, H. B. Schlegel, G. E. Scuseria, M. A. Robb, J. R. Cheeseman, G. Scalmani, V. Barone, B. Mennucci, G. A. Petersson, H. Nakatsuji, M. Caricato, X. Li, H. P. Hratchian, A. F. Izmaylov, J. Bloino, G. Zheng, J. L. Sonnenberg, M. Hada, M. Ehara, K. Toyota, R. Fukuda, J. Hasegawa, M. Ishida, T. Nakajima, Y. Honda, O. Kitao, H. Nakai, T. Vreven, J. A. Montgomery Jr, J. E. Peralta, F. Ogliaro, M. Bearpark, J. J. Heyd, E. Brothers, K. N. Kudin, V. N. Staroverov, R. Kobayashi, J. Normand, K. Raghavachari, A. Rendell, J. C. Burant, S. S. Iyengar, J. Tomasi, M. Cossi, N. Rega, J. M. Millam, M. Klene, J. E. Knox, J. B. Cross, V. Bakken, C. Adamo, J. Jaramillo, R. Gomperts, R. E. Stratmann, O. Yazyev, A. J. Austin, R. Cammi, C. Pomelli, J. W. Ochterski, R. L. Martin, K. Morokuma, V. G. Zakrzewski, G. A. Voth, P. Salvador, J. J. Dannenberg, S. Dapprich, A. D. Daniels, Ö. Farkas, J. B. Foresman, J. V. Ortiz, J. Cioslowski and D. J. Fox, Gaussian 09 (Revision E.01), Gaussian Inc., Wallingford CT, 2013.

